AIChE

# Influence of Elevated Pressure and Particle Lyophobicity on Hydrodynamics and Gas–Liquid Mass Transfer in Slurry Bubble Columns

**Vinit P. Chilekar, John van der Schaaf, and Ben F. M. Kuster**
Laboratory of Chemical Reactor Engineering, Eindhoven University of Technology, Eindhoven, The Netherlands

**Johan T. Tinge**
Industrial Chemicals Chemistry and Technology, DSM Research, P.O. Box 18, 6160 MD Geleen, The Netherlands

**Jaap C. Schouten**
Laboratory of Chemical Reactor Engineering, Eindhoven University of Technology, Eindhoven, The Netherlands

*DOI 10.1002/aic.11987*
*Published online September 29, 2009 in Wiley InterScience (www.interscience.wiley.com).*

*This article reports on the influence of elevated pressure and catalyst particle lyophobicity at particle concentrations up to 3 vol % on the hydrodynamics and the gas-to-liquid mass transfer in a slurry bubble column. The study was done with demineralized water (aqueous phase) and Isopar-M oil (organic phase) slurries in a 0.15 m internal diameter bubble column operated at pressures ranging from 0.1 to 1.3 MPa. The overall gas hold-up, the flow regime transition point, the average large bubble diameter, and the centerline liquid velocity were measured along with the gas–liquid mass transfer coefficient. The gas hold-up and the flow regime transition point are not influenced by the presence of lyophilic particles. Lyophobic particles shift the regime transition to a higher gas velocity and cause foam formation. Increasing operating pressure significantly increases the gas hold-up and the regime transition velocity, irrespective of the particle lyophobicity. The gas–liquid mass transfer coefficient is proportional to the gas hold-up for all investigated slurries and is not affected by the particle lyophobicity, the particle concentration, and the operating pressure. A correlation is presented to estimate the gas–liquid mass transfer coefficient as a function of the measured gas hold-up:* $k_l a_l/\varepsilon_g = 3.0\sqrt{Du_b/d_b^3}\ s^{-1}$. © 2009 American Institute of Chemical Engineers *AIChE J*, 56: 584–596, 2010

*Keywords: slurry bubble column, high pressure, gas hold-up, mass transfer, hydrodynamics, regime transition, pressure fluctuations, liquid velocity, electrolyte, lyophobicity*

## Introduction

Slurry bubble column (SBC) reactors are widely used in the chemical industry as efficient gas–liquid–solid contactors, for example, for aerobic fermentation, hydrogenation, oxidation reactions, and gas–liquid Fischer-Tropsch synthesis. Advantages of an SBC reactor over other reactors are its

Correspondence concerning this article should be addressed to J. C. Schouten at j.c.schouten@tue.nl.
Current address of Vinit P. Chilekar: Polymer Process Development Group GKE/D, Global Polymer Research, BASF SE, Ludwigshafen, Germany.

**Table 1. Overview of Literature Studies on Bubble Columns and Slurry Bubble Columns at Elevated Pressure**

| Authors | System | Operating Conditions | Techniques |
|---|---|---|---|
| **Bubble columns** | | | |
| Behkish et al.[3] | $H_2$, CO, $N_2$, $CH_4$-Isopar M and hexane mixtures $D_c = 0.316$ m, $H = 2.8$ m spider sparger | $P = 0.17$–$0.8$ Mpa<br>$T = 293$ K<br>$u_g = 0.08$–$0.20$ m s$^{-1}$ | Gas absorption in a closed circulating system |
| Dewes and Schumpe[4] | Air-$H_2O$, 0.8 M sodium sulphate, xanthum gum solutions-kiesel-guhr, alumina $D_c = 0.115$ m, $H = 1.37$ m perforated plate (7 holes of 1 mm) | $P = 0.1$–$0.8$ MPa<br>$T = 298$ K<br>$u_g = 0.03$–$0.08$ m s$^{-1}$ | Pressure method |
| Idogawa et al.[5] | $H_2$, He, air/$H_2O$, $CH_3OH$, $C_2H_5OH$, acetone, aqueous alcohol solutions | $P = 0.1$–$5$ MPa<br>$T = 293$ K<br>$u_g = 0.0005$–$0.05$ m s$^{-1}$ | – |
| Jiang et al.[6] | $N_2$-paratherm NF, $D_c = 0.0508$ m ring sparger | $P = 0.1$–$12.2$ MPa<br>$T = 298$ K<br>$u_g = 0.025$–$0.075$ m s$^{-1}$ | Gas absorption |
| Jordan et al.[7] | $O_2$-water, ethanol, 1-butanol, toluene, $D_c = 0.11$ m, $H = 1.37$ m, several perforated plates | $P = 0.1$–$1.0$ MPa<br>$T = 293$ K<br>$u_g = 0.15$ m s$^{-1}$ | Oxygen absorption |
| Kojima et al.[8] | $N_2/O_2$-water $N_2/O_2$ solution of enzyme, $D_c = 0.045$ m, single nozzle with different diameters | $P = 0.1$–$1.1$ MPa<br>$T = 290$–$300$ K<br>$u_g = 0.0005$–$0.15$ m s$^{-1}$ | Height measurement method, oxygen absorption |
| Lau et al.[9] | Air-paratherm NF, $D_c = 0.1016$ m perforated plate (120 holes of 1.5 mm) | $P = 0.1$–$4.24$ MPa<br>$T = 298$, 365 K<br>$u_g = 0.019$–$0.39$ m s$^{-1}$<br>$u_l = 0.008$–$0.0032$ m s$^{-1}$ | Oxygen absorption |
| Lemoine et al.[10] | $N_2$, air-toluene, toluene + benzoic acid + benzaldehyde, $H_2O$ $D_c = 0.316$ m, $H = 2.8$ m spider sparger | $P = 0.182$–$0.82$ MPa<br>$T = 298$ K<br>$u_g = 0.056$–$0.15$ m s$^{-1}$ | Gas absorption, Dynamic gas disengaging, manometeric method |
| Letzel et al.[11] | $N_2$-water, $D_c = 0.15$ m, $H = 1.3$ m, perforated plate (200 holes of 0.5 mm) | $P = 0.1$–$1.3$ MPa<br>$T = 293$ K<br>$u_g = 0.01$–$0.30$ m s$^{-1}$ | Overflow method, Pressure step method |
| Oyevaar et al.[12] | $CO_2/N_2$-water, $CO_2/N_2$-DEA, $D_c = 0.085$ m, $H = 0.63$ m, perforated plate (16 holes of 0.5 mm) | $P = 0.1$–$1.85$ Mpa<br>$T = 293$ K<br>$u_g = 0.01$–$0.09$ m s$^{-1}$ | Chemical absorption height difference method |
| Oyevaar et al.[13] | $CO_2/N_2$-water, $CO_2/N_2$-DEA, $D_c = 0.085$ m, $H = 0.81$ m, perforated plate (21 holes of 0.4 mm), sintered porous plate | $P = 0.15$–$8$ MPa<br>$T = 293$ K<br>$u_g = 0.01$–$0.10$ m s$^{-1}$ | Chemical absorption height difference method |
| Pohorecki et al.[14] | $N_2$/water, $D_c = 0.304$ m, $H = 4$ m, spargers with geometries | $P = 0.1$–$1.1$ MPa<br>$T = 303$–$433$ K<br>$u_g = 0.013$–$0.035$ m s$^{-1}$ | Photography |
| Reilly et al.[15] | Air, $N_2$, He, Ar, $CO_2$/Isopar G, Isopar M, $D_c = 0.15$ m, $H = 2.7$ m | $P = 0.1$–$1.1$ MPa<br>$T = 293$ K<br>$u_g = 0.006$–$0.23$ m s$^{-1}$ | Pressure method |
| Stegeman et al.[16] | $N_2/CO_2$-DEA, ETG, water, $D_c = 0.156$ m, $H = 0.64$ m, perforated plate (284 holes of 0.4 mm) | $P = 0.1$–$6.6$ MPa<br>$T = 293$ K<br>$u_g = 0.01$–$0.05$ m s$^{-1}$ | Chemical absorption |
| Tarmy et al.[17] | $N_2$-*n*Heptane, $D_c = 0.61$ m single orifice nozzle | $P = 0.12$–$0.62$ MPa<br>$T = 298$ K<br>$u_g$ upto 0.12 m s$^{-1}$ | Gas absorption |
| Urseanu et al.[18] | $N_2$/tellus oil, glucose solution, $D_c = 0.15, 0.23$ m, $H = 1.22$ m, perforated plate (19 holes of 10 mm) | $P = 0.1$–$1$ MPa<br>$T = 293$ K<br>$u_g = 0.001$–$0.30$ m s$^{-1}$ | Overflow method |
| Vafopulos et al.[19] | $N_2/O_2$-water, $D_c = 0.4$ m, $H = 1.46$ m, porous plate (90 mm) capillary tube of 3 mm | $P = 0.1$–$2.5$ MPa<br>$T = 293$ K<br>$u_g = 0.0067$–$0.026$ m s$^{-1}$ | Physical absorption, liquid concentration photography |
| Wilkinson et al.[20] | Air-sodium sulphite, $D_c = 0.158$ m, $H = 1.4$ m, perforated plate (19 holes of 10 mm) | $P = 0.1$–$2$ MPa<br>$T = 293$ K<br>$u_g = 0.01$–$0.15$ m s$^{-1}$ | Photography, uncatalyzed oxidation of sodium sulfite |
| Yang and Fan[21] | $H_2$/CO, $N_2$-liquid paraffin-silica gel powder, $D_c = 0.037$ m | $P = 1$–$5$ MPa<br>$T = 293$–$523$ K<br>$u_g < 0.02$ m s$^{-1}$<br>$\varepsilon_s = 5$–$20$ vol % | Gas absorption |
| **Slurry bubble columns** | | | |
| Bethkish et al.[22] | $N_2$, He-Isopar M-alumina, $D_c = 0.316$ m, $H = 2.8$ m, spider sparger | $P = 0.7$–$3.0$ MPa<br>$T = 300$–$453$ K<br>$u_g = 0.07$–$0.39$ m s$^{-1}$<br>$\varepsilon_s = 0$–$20$ vol % | Gas absorption, manometric method |

**Table 1. (*Continued*)**

| Authors | System | Operating Conditions | Techniques |
|---|---|---|---|
| Deckwer et al.[23] | $N_2$-wax-alumina, $D_c = 0.1$ m, $H = 2.3$ m, sintered plate | $P = 0.4$ MPa<br>$T = 523$ K<br>$u_g = 0.0044$–$0.034$ m s$^{-1}$<br>$\varepsilon_s = 0$–$1.21$ vol % | Gas absorption, pressure method |
| Inga and Morsi[24] | $H_2$, CO, $CH_4$, $N_2$-hexanes-iron oxides, $D_c = 0.316$ m, $H = 2.8$ m, spider sparger | $P = 0.126$–$0.787$ MPa<br>$T = 298$ K<br>$u_g = 0.06$–$0.35$ m s$^{-1}$<br>$\varepsilon_s = 0$–$21.76$ vol % | Gas absorption, manometric method |
| Luo et al.[25] | $N_2$-Paratherm NF-Alumina, $D_c = 0.102$ m, $H = 2.8$ m, perforated plate | $P = 0.1$–$2.86$ MPa<br>$T = 298$ K<br>$u_g = 0.04$–$0.334$ m s$^{-1}$<br>$\varepsilon_s = 0$–$19.1$ vol % | Gas absorption, pressure method |

relatively simple construction, low investment and operating costs, and excellent heat and mass transfer characteristics.

The design of an industrial SBC reactor requires a thorough understanding of its hydrodynamics and mass transfer characteristics which are influenced by the physical properties of the gas, the liquid, and the solid phases, the operating parameters (pressure, temperature), and the design parameters (column diameter, distributor, internals). The gas hold-up is the most important hydrodynamic parameter governing the SBC reactor design.[1,2] All other design parameters, such as the mass transfer coefficient and the axial dispersion coefficient, can be correlated to the gas hold-up.

Industrial SBCs are usually operated at elevated pressure and temperature to get a high productivity. At elevated operating pressure, due to the increased gas density, the hydrodynamics and the gas-to-liquid mass transfer differ from that at atmospheric pressure. It is, therefore, important to investigate the influence of elevated pressure on the hydrodynamics and the mass transfer in slurry bubble columns. The presence of catalyst particles also influences the hydrodynamics, mainly by increasing the viscosity of the slurry at higher slurry concentrations and also due to the different wetting properties (i.e., lyophobicity/lyophilicity) of the particles with the liquid. Lyophobic particles having bad wetting characteristics when compared with lyophilic particles will tend to be present at the gas–liquid interface and would influence the bubble coalescence behavior leading to changed hydrodynamics. In industrial columns with actual reaction systems, there are reactants, (by-)products, and sometimes also a solvent present which adds to the changed hydrodynamics of the SBC. The presence of an electrolyte in a slurry with catalyst particles at elevated pressure could also significantly influence the hydrodynamics and the rate of gas-to-liquid mass transfer.

In this article, the influence of the operating pressure, the surface lyophobicity of the particles, and the influence of electrolytes on the hydrodynamics and the mass transfer in a laboratory scale SBC is presented. The influences were studied both in the homogeneous flow regime and in the churn-turbulent flow regime. The hydrodynamic parameters presented are the overall gas hold-up, the flow regime transition, the average large bubble size, and the centerline liquid velocity. Also the gas–liquid mass transfer coefficient is given.

## Literature Survey

Several investigations studying the effect of pressure on hydrodynamics and mass transfer in (slurry) bubble columns have been reported in the literature, Table 1. The overview shows that most of the early research focused on the effect of pressure in the homogeneous flow regime.[4,6,8,9,12–14,16,19,21,23] Vafopulos et al.[19] were amongst the first to carry out experiments at higher pressure, but ended up showing that there was no effect of pressure on the gas hold-up, mass transfer coefficient, nor on the interfacial area at lower superficial gas velocities ($u_g < 0.026$ m s$^{-1}$). However, more recent research (Table 1) showed that the gas hold-up, the mass transfer coefficient, and the gas–liquid interfacial area increase considerably with increasing pressure.

Oyevaar et al.[12] showed that the increase in the gas hold-up is larger for organic liquids than for demineralized water. Kojima et al.[8] showed that the interfacial area increases with increasing pressure and that this effect is larger with decreasing diameter of the holes in the gas distributor. These studies were only limited to the homogeneous flow regime.

Recent studies mainly were focused on the churn-turbulent flow regime with superficial gas velocities closer to the operating conditions of a Fischer-Tropsch reactor used for converting synthesis gas into liquid fuels.[7,11,15,18,20,22,24,25]

Letzel et al.[11] showed that with an increase in operating pressure, the flow regime transition occurs at a higher transition gas hold-up which results from a decrease in the rise velocity of the large gas bubbles in the churn-turbulent flow regime. Some researchers studied slurries at elevated pressure in comparison with the pure liquids. Luo et al.[25] and Behkish et al.[22] used alumina particles in organic liquids, whereas Inga and Morsi[24] used iron oxide particles in organic liquids. The particle wettability and the slurry concentration have a large influence on SBC behavior at atmospheric pressure, but the behavior of slurry particles under the influence of higher pressure is still unknown. Tinge et al.[26] reported the influence of the addition of small activated carbon particles on the gas hold-up for various pressures in a down flow jet loop reactor. At low pressure, the presence of a low content of activated carbon particles increases the gas hold-up, whereas a higher solid content reduces the gas hold-up sharply. The positive influence of carbon fines on the gas hold-up diminishes at higher gas pressure. The degree of lyophobicity of the particles influences the hydrodynamics as shown by Ruthiya

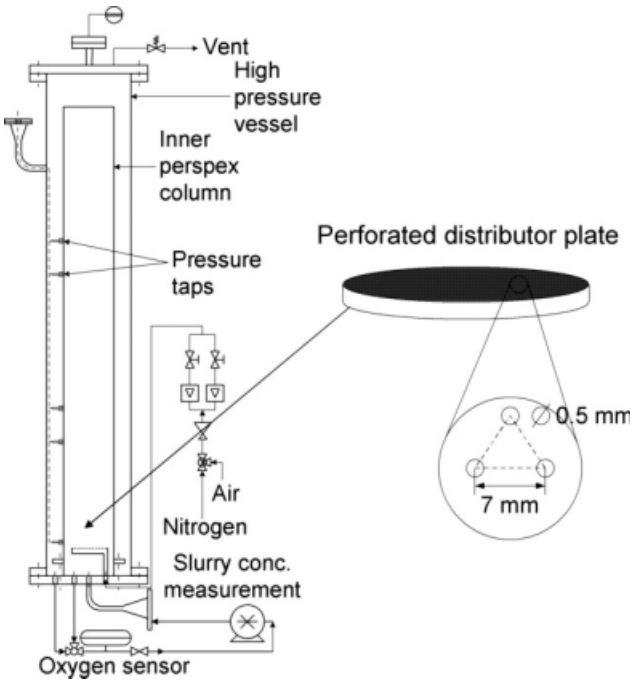


**Figure 1. Schematic description of the high pressure slurry bubble column setup and the gas distributor design.**

et al.[27] This effect can be different for aqueous and organic liquids as the particles have different lyophobicities in these liquids based on the liquids' varying surface tension.

## Experimental Setup

The experimental setup is schematically depicted in Figure 1; Letzel and Stankiewicz[28] for more details. The internal diameter of the SBC is 0.15 m, it is 1.4 m high and has a 0.10 m diameter perforated plate gas distributor placed in the center of the column at 0.085 m from its bottom (Figure 1). Demineralized water and organic oil (Isopar M, ExxonMobil) were used as the liquid phase. The properties of the gases, liquids, and solids are given in Table 2.

In demineralized water, the activated carbon particles are lyophobic and the silica particles are lyophilic, whereas in Isopar M, these particles are equally lyophilic,[29] as determined from the heat of immersion of the particles ($\Delta H$) in the respective liquids, shown in Table 2. Slurry concentrations ranged from 0 to 3 vol %. Sodium gluconate was used as the electrolyte in the experiments to reduce the surface tension in the demineralized water system. All experiments were carried out at ambient temperature (19–23°C) and operating pressures from 0.1 to 1.3 MPa. All the gas flow rates mentioned in this article are volumetric flows unless otherwise mentioned.

Air was added to the main nitrogen stream to introduce a step change in the oxygen concentration of the inlet gas from 0 to 5 vol % for all mass transfer experiments. The slurry was sampled at 0.3 m from the bottom of the column, passed through an oxygen sensor (Orbisphere, 3600), and then recycled to the bottom of the SBC. For the mass transfer measurements, it was assumed that there is no radial variation and the measured mass transfer is the average value over the cross section of the SBC. The oxygen sensor response time was determined for all slurries and operating pressures, and varied between 0.05 and 0.07 $s^{-1}$.

Five differential pressure sensors (Druck: LPM 9381) were used to measure the gas hold-up in the column. The sensors were connected at heights of 0.1, 0.4, 0.7, 0.9, and 1.1 m from the bottom of the column using 1 mm inner diameter metal capillaries. Thorat et al.[30] showed that the axial gas hold-up increases from the sparger upto a H/D ratio of two, and beyond this H/D ratio, the gas hold-up is relatively constant for higher H/D ratios of the gas–liquid dispersion. The gas hold-up is hence assumed to be approximately constant above 0.4 m (i.e., above a H/D ratio of 2.5) and is considered as representative for the gas hold-up in SBCs. This gas hold-up is, therefore, reported as the overall gas hold-up in this article. The gas hold-up between sensor positions 0.1 and 0.4 m is at most 5% lower in the homogeneous flow regime and 15% lower in the churn-turbulent flow regime when compared with the overall gas hold-up. Hence, the overall gas hold-up is overestimated by 2 and 6% in the homogeneous flow regime and churn-turbulent flow regime, respectively.

Five differential pressure sensors (Kulite pressure transducers; range: 1.7 bar differential; accuracy: 0.25 % of full scale) were used to measure the fast pressure fluctuations in the column for the estimation of the regime transition point and the average large bubble diameter by spectral analysis of the dynamic pressure fluctuations.[27,31] These fast pressure fluctuations were measured at a sampling frequency of 100 Hz and were filtered at a frequency of 50 Hz.

The upward liquid velocity was measured using a Pitot tube placed in the center of the column. The Pitot tube was pointing downwards in the center of the column and the

**Table 2. Physical Properties of Used Gases, Liquids, and Solids**

| Gas | $N_2$ | Air |
|---|---|---|
| $M_A$, kg k $mol^{-1}$ | 28.013 | 28.85 |
| $T_c$, K | 126.2 | 133.3 |
| $P_c$, MPa | 3.39 | 3.9 |
| $\upsilon_A$, $m^3$ k $mol^{-1}$ × 1000 | 31.76 | 20.1 |
| Liquid | Demineralized water | Isopar M |
| $M_B$, kg k $mol^{-1}$ | 18 | 192 |
| $\rho_L$ (298 K), kg $m^{-3}$ | 998 | 783 |
| $\mu_L$ (298 K), mPa s | 1.1 | 2.7 |
| $\sigma_L$ (298 K), N $m^{-1}$ | 0.072 | 0.027 |
| $D_{O_2}$(298 K), $m^2$ $s^{-1}$ | $2.2 \times 10^{-9}$ | $1.4 \times 10^{-9}$ |
| Solid particles | Carbon | Silica |
| Supplier code | 43242, Norit NV | G-5268, Promeks |
| $\rho_s$, kg $m^{-3}$ | 1300 | 2130 |
| $d_p$, $\mu$m | 30 | 44 |
| $S_{BET}$, $m^2$ $g^{-1}$ | 850 | 485 |
| Pore width (nm) | 9.2 | 8.6 |
| $V_{s,p}$, ml $g^{-1}$ | 1.60 | 1.63 |
| $\varepsilon_p$, dimensionless | 0.65 | 0.85 |
| $\Delta H_{aqueous}$, mJ $m^{-2}$ | −54 | −201 |
| $\Delta H_{organic}$, mJ $m^{-2}$ | −126 | −103 |

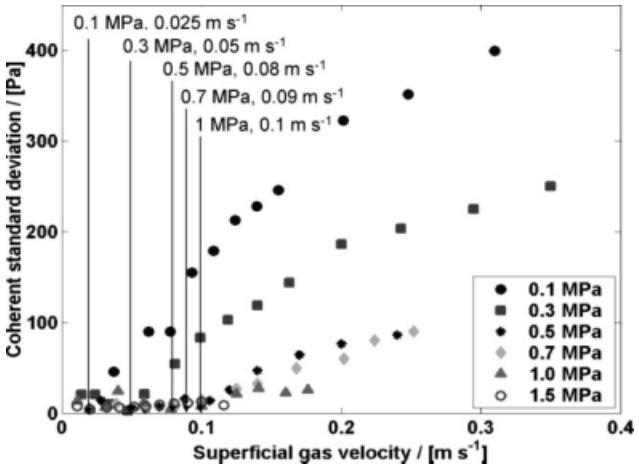


**Figure 2. Coherent standard deviation of the pressure fluctuations measured in the slurry bubble column in Figure 1 at elevated pressures to determine the flow regime transition velocity as described by Ruthiya et al.[29]**

$N_2$-demineralized water system was used for experiments at operating pressures of 0.1, 0.3, 0.5, 0.7, 1.0 and 1.5 MPa.

reference tube was placed just 3 mm below the measurement point. The Pitot tube measured the pressure drop generated by the impact pressure of the upward flowing liquid in the center of the column. The assumption used in these measurements is that the horizontal component of the liquid velocity is negligible when compared with the vertical component. Thus only the vertical velocity is considered here. If this assumption is not correct, then the measured pressure drop needs to be corrected for the horizontal liquid velocity component by also measuring the pressure drop with the Pitot tube pointing in upward direction, which was, however, not possible in the present setup configuration.

The measured pressure difference is recorded by the differential pressure transducer placed outside the high pressure vessel. The interstitial liquid velocity is obtained as:

$$V_l = \sqrt{\frac{2\Delta P}{\rho_l(1-\varepsilon_g)}} \tag{1}$$

where $V_l$ the interstitial centerline liquid velocity, $\Delta P$ the pressure drop measured by the differential pressure transducer, $\rho_l$ the density of the slurry, $\varepsilon_g$ the gas hold-up at that superficial gas velocity. The gas hold-up $\varepsilon_g$ used in calculating $V_l$ is the average gas hold-up and not the local, radial gas hold-up as we were unable to measure this local gas hold-up. The average gas hold-up is lower than the local gas hold-up in the centre of the SBC, yielding, therefore, an interstitial centerline liquid velocity which is estimated to be approximately 20% lower than its ''true'' value, using the radial voidage profile as determined by Rice and Geary (1990).[32]

The radial profile is given by: $\varepsilon_{g,r}/\varepsilon_g = (m+2)/m \cdot (1-(r/R)^m)$ So for $r = 0$, $\varepsilon_g = 1 + 2/m$. Rice and Geary[32] state that $m$ should lie between five (heterogeneous) and eight (homogeneous). For $m = 5$, $\varepsilon_g$ is 40% higher, for $m = 8$, 25%. If the gas hold-up is at maximum 0.5, then the centerline liquid velocity is underestimated by a factor $((1-0.5)/(1-0.7))^{0.5} = 1.3$, for $m = 8$ a factor $((1-0.5)/(1-0.625))^{0.5} = 1.15$. All lower holdups will have a lower correction factor. The average between the correction factors is 22%, hence a conservative correction factor of 20% is used in this article.

## Results and Discussion

### *Regime transition velocity*

The regime transition velocity was determined using the coherent standard deviation of the measured pressure time series as explained by Ruthiya et al.[27] In this technique, the coherent standard deviation obtained from a spectral analysis of the dynamic pressure fluctuations in the SBC is calculated and plotted for all the superficial gas velocities. The coherent standard deviation is very close to zero for superficial gas velocities in the homogeneous flow regime. As the superficial gas velocity increases, the transition from the homogeneous to the heterogeneous flow regime is indicated by a sharp rise in the coherent standard deviation, corresponding to the formation of large bubbles. The velocity at which the coherent standard deviation increases sharply is designated as the regime transition velocity. This technique was developed in bubble columns operated at atmospheric pressure,[27] and in this article, it is applied for SBCs operating at elevated pressure. The coherent standard deviation measured in the demineralized water (nonslurry) system at elevated pressure is shown in Figure 2. At 0.1 MPa, for $u_g = 0.25$ m s$^{-1}$, there is a steep increase of the coherent standard deviation, hence this is the regime transition velocity for 0.1 MPa. Similarly, for higher pressures of 0.3, 0.5, 0.7, 1.0, and 1.5 MPa, the regime transition velocities are identified as denoted in Figure 2. It is seen that with increasing operating pressure the regime transition velocity increases, thus indicating that the operating pressure stabilizes the homogeneous flow regime and delays the transition to the churn-turbulent flow regime.

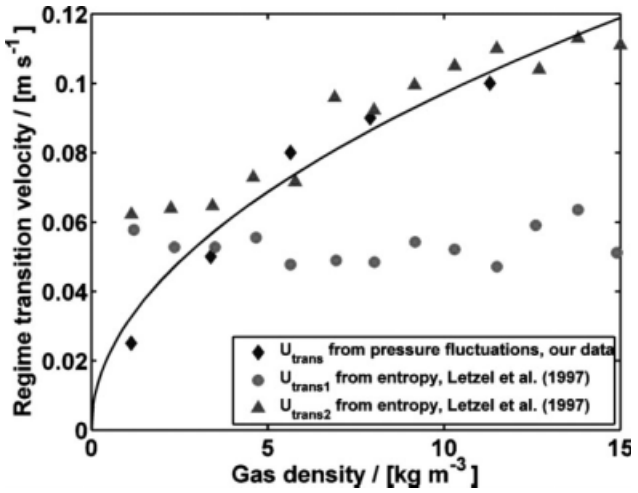


**Figure 3. Comparison of the flow regime transition velocity of our data and the data published by Letzel et al.[11] at elevated pressure for a demineralized water system.**

The solid black line shows that $u_{trans} \alpha \sqrt{\rho_g}$.

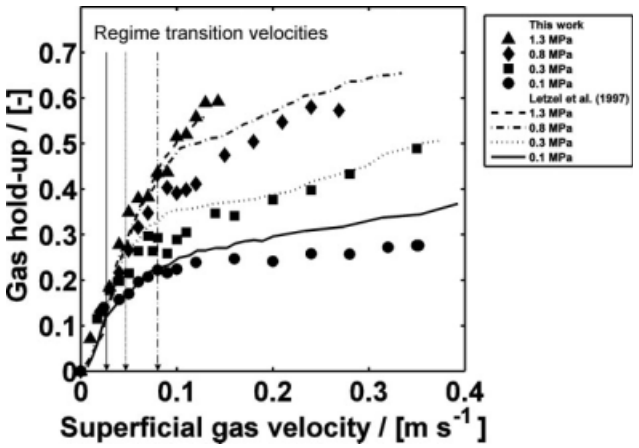


**Figure 4. The gas hold-up for pressures from 0.1 to 1.3 MPa for demineralized water.**

The solid lines are the gas hold-up data presented by Letzel et al.[33] using the overflow method. The solid markers are data points measured by the pressure drop method in this work. The regime transition velocities[27] are indicated by vertical lines.

In Figure 3, the flow regime transition velocity is plotted against the gas density. The regime transition velocity does not increase linearly with the operating pressure. Letzel et al.[11] used the Kolmogoroff entropy obtained from chaos analysis of pressure time series, to determine the regime transition velocity. Based on the Kolmogoroff entropy, they defined two transition points marking the beginning and the end of the transition region, respectively. At the first transition point, bubbles larger than 4 mm are formed and at the second transition point large bubbles rising with a higher rise velocity are formed in the bubble column. Both these transition points measured by Letzel et al.[11] are compared with the single regime transition point obtained by our measurement technique in Figure 3. At the transition point measured by our technique, bubbles larger than 6 mm are observed in the bubble column, in agreement with Ruthiya et al.[27] This transition point is close to the value of the second transition point defined by Letzel et al.[11] At lower gas densities, our regime transition point is lower than the regime transition points determined by Letzel et al.[11] However, at high gas densities, our regime transition points completely overlap the second transition point determined by Letzel et al.[11] The results shown in Figures 2 and 3 suggest that this measurement technique based on the coherent standard deviation of pressure fluctuations is a useful technique to determine the flow regime transition point at elevated pressure. It is strongly correlated to the existence of large bubbles from a physical point of view.

### *Gas hold-up*

The gas hold-up for the demineralized water system is shown in Figure 4 at operating pressures of 0.1, 0.3, 0.8, and 1.3 MPa. The gas hold-up data in the homogeneous flow regime resemble the data from Letzel et al.,[33] which were obtained in the same experimental setup. However, in the churn-turbulent flow regime the gas hold-up is at most 20% lower than the data of Letzel et al.[33] as they measured the volume of the liquid overflow to estimate the gas hold-up, which overestimates the gas hold-up due to the increased overflow by the sloshing motion of the liquid, especially in the churn-turbulent flow regime. The data presented in this article is based on the measurement of the pressure drop in the column and is thus unbiased towards the effect of sloshing.

In Figure 5, the gas hold-up for the carbon-demineralized water slurries is shown as a function of the superficial gas velocity for pressures of 0.1 and 0.3 MPa. At higher pressures, severe foaming made stable operation of the column impossible beyond 0.1 m $s^{-1}$ superficial gas velocity. At 0.1 MPa, the gas hold-up in the homogeneous flow regime for the carbon particle concentration of 0.7 vol % is almost equal to the demineralized water gas hold-up. There is a significant increase in the gas hold-up in the churn-turbulent flow regime due to the influence of the activated carbon particles. Kluytmans et al.[34] observed the same increase in a two-dimensional SBC. Ruthiya et al.[35] observed an increase in the gas hold-up from 0 to 0.14 vol % carbon particle concentration; above 0.14 vol % the gas hold-up decreased. The increase in the gas hold-up can be a result of inhibition of gas bubble coalescence: lyophobic particles adhere to the gas–liquid interface and prevent the formation and draining of the thin liquid film formed between the colliding small bubbles. Therefore, the number of small bubbles is higher in the churn-turbulent flow regime and the gas hold-up correspondingly increases. The transition from the homogeneous flow regime to the churn-turbulent flow regime is also delayed by coalescence inhibition, which is especially discernable at a pressure of 0.3 MPa. For the carbon particle concentration of 0.7 vol %, the coalescence is completely inhibited and only the homogeneous flow regime could be obtained. Foaming was observed at high gas velocities, at times accompanied by slugging behavior. This foaming phenomenon is a characteristic feature of slurry bubble columns with lyophobic particles operated at elevated pressure.

Figure 6 compares the gas hold-up of the 0.7 vol % silica-demineralized water slurry for pressures of 0.1, 0.3, 0.8, and

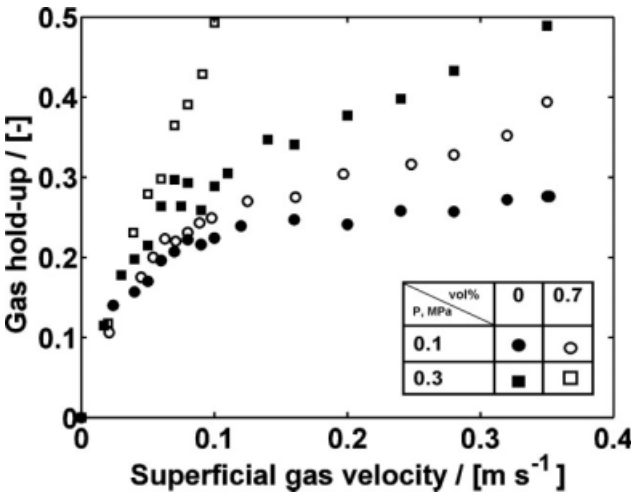


**Figure 5. Influence of activated carbon particles on the gas hold-up for different superficial gas velocities at pressures of 0.1 and 0.3 MPa.**

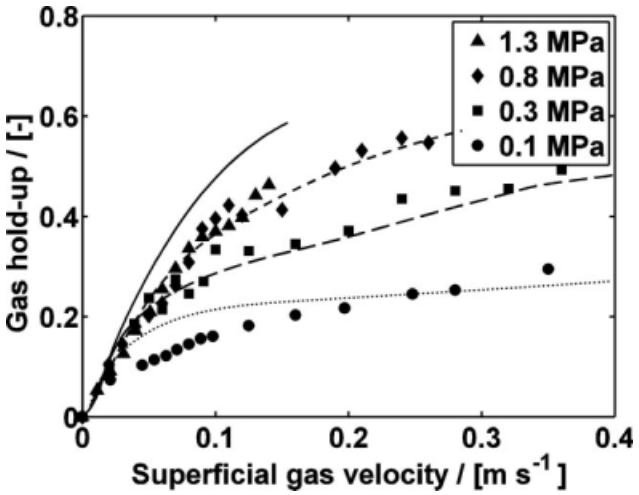


**Figure 6. Gas hold-up for a 0.7 vol % silica-demineralized water slurry at pressures from 0.1 to 1.3 MPa.**

The line represents the gas hold-up for demineralized water.

1.3 MPa. The lyophilic silica particles do not adhere to the gas–liquid interface and foaming is not observed. At pressures of 0.1 and 1.3 MPa, the gas hold-up is slightly lower than for demineralized water; no significant influence is observed at pressures of 0.3 and 0.8 MPa.

In Figure 7a, the gas hold-up is shown for the electrolyte-demineralized water system at elevated pressure. Sodium gluconate is the electrolyte used in the experiments, as mentioned earlier. The sodium gluconate dissociates in water and an electrical double layer forms at the gas–liquid interface. The accumulation of dissociated ions at the interface creates surface tension gradients over the gas–liquid interfacial area decreasing the total surface tension of the electrolyte solution. This decrease in surface tension with addition of sodium gluconate was also observed by Kluytmans et al.[34]

The concentration of 0.05 M electrolyte only decreases the surface tension from 72 mN $m^{-1}$ to 68 mN $m^{-1}$. This negligible change in surface tension gives similar gas hold-up profiles as for pure demineralized water. With 0.1 M electrolyte concentration, the surface tension of the liquid phase decreases to 61 mN $m^{-1}$, leading to a considerable increase in the gas hold-up already in the homogeneous flow regime. The rate of increase of the gas hold-up is higher, which also supports the fact that the electrolyte directly reduces the coalescence of the small bubbles. The rate of increase of the gas hold-up in the homogeneous flow regime increases with operating pressure. Beyond the regime transition point, it was difficult to operate the column in a stable mode. At these higher gas velocities, the column was overflowing due to severe foaming in the liquid. In Figure 7b, the gas hold-up profiles for the influence of the carbon slurries in electrolyte solutions are shown. In this type of systems, the combination of electrolyte and activated carbon particles increases the gas hold-up in the homogeneous flow regime. Therefore, there is a steep increase in the gas hold-up for all higher operating pressures. Here again it was difficult to operate the column in a stable hydrodynamic regime after the transition point or even at superficial gas velocities higher than 0.05 m $s^{-1}$.

In Figure 8, the gas hold-up is shown as a function of the gas velocity for carbon-Isopar M slurries and silica-Isopar M slurries for particle concentrations of 0.7 and 2.8 vol %. The negligible influence of lyophilic particles on the gas hold-up is confirmed. Reilly et al.[15] already found that in the churn-turbulent flow regime, the gas hold-up of Isopar M is higher than that of demineralized water. The lower surface tension of Isopar M increases the bubble break-up rate and the higher viscosity reduces the bubble coalescence (increased film drainage time[36]), which increases the number of small bubbles. Accordingly, Isopar M is inherently prone to foaming due to its lower surface tension. The presence of particles does not lead to additional foaming.

In Figure 8a, the gas hold-up of silica-Isopar M slurries is shown as a function of the gas velocity at various operating

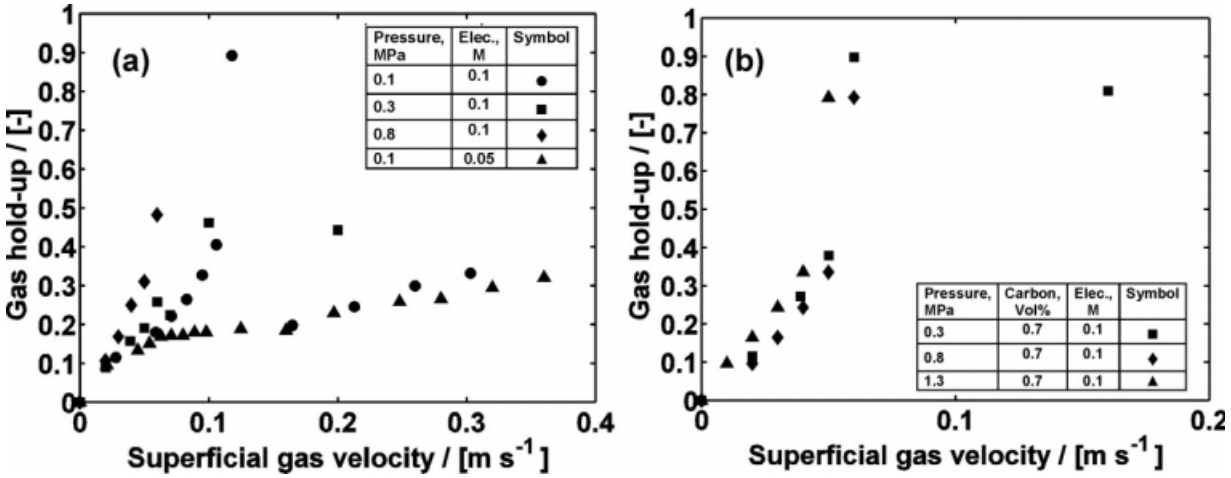


**Figure 7. Gas hold-up profiles for different systems in demineralized water at various pressures: (a) impact of concentration of electrolyte in demineralized water, (b) impact of addition of electrolyte and activated carbon particles to demineralized water.**

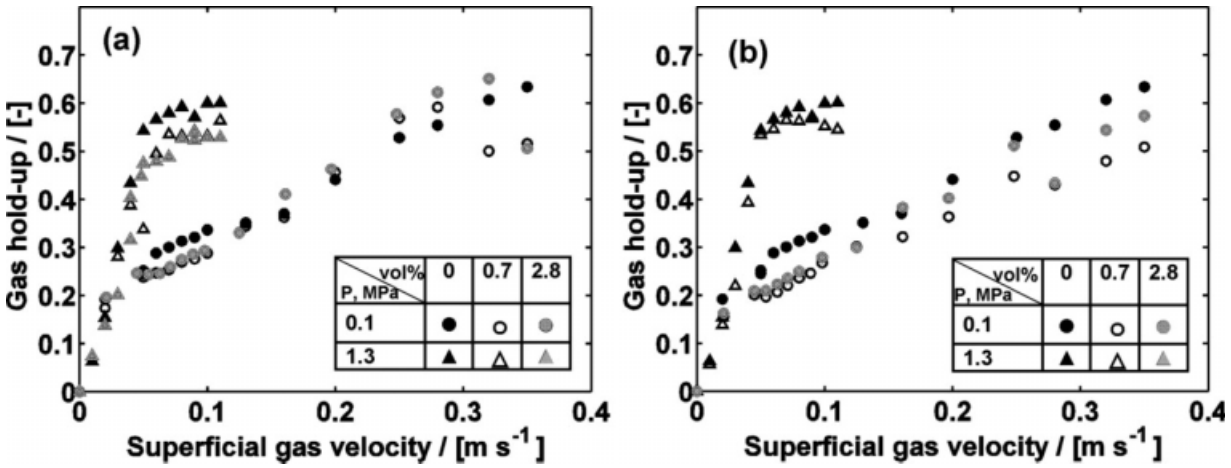


**Figure 8. Gas hold-up for (a) silica-Isopar M slurries, and (b) carbon-Isopar M slurries at pressures from 0.1 to 1.3 MPa.**

pressures. At atmospheric pressure, the gas hold-up decreases only slightly with the silica particle concentration increasing from 0 to 0.7 vol %, comparable to the silica-demineralized water slurries. At 1.3 MPa pressure, a similar slight decrease in the gas hold-up is observed. This is expected for the silica particles as they are almost equally lyophilic to demineralized water as to Isopar M (Table 2). The lyophilicity of the activated carbon particles to Isopar M is comparable to the silica particles. Consequently, the gas hold-up of the carbon-Isopar M slurries closely resembles the gas hold-up of the silica-Isopar M slurries, Figure 8b.

### *Mechanism for bubble coalescence at the gas distributor in the presence of particles*

The influence of the particles on the gas hold-up and on the regime transition point can be explained by the formation of bubbles at the gas distributor. In Figure 9, schematic diagrams for a noncoalescing system and for a coalescing system are shown. At the orifice in the gas distributor, as the gas flows into the bubble, the bubble grows in size, being still attached to the gas distributor. As soon as the buoyancy force is larger than the surface tension force, the bubble detaches from the distributor.

The gas flow through the orifice determines the frequency of bubble formation for a constant bubble size. The diameter of the bubble formed at the distributor orifice can be calculated from the force balance at the orifice. In case of a low gas flow, single bubbles detach and rise without interaction with the leading or trailing bubbles forming a chain. As the gas flow increases, the frequency of bubble formation increases. The bubbles interact with the leading bubbles and collide with the bubbles as they rise. In case of a noncoalescing system, this collision of small bubbles does not result into coalescence as is shown in Figure 9a. The presence of particles or surface active agents increases the coalescence time which can be higher than the time taken by the two bubbles to drift away from each other as they rise. In case of a coalescing system, the two colliding bubbles instantly coalesce to form a large bubble. The large bubble then rises faster than the small bubbles. At very high gas flow through the distributor orifice, the impact of the trailing gas bubble is higher on the leading bubbles, leading to instant coalescence of bubbles. Instead of formation of single bubbles, a jet is formed which breaks up to form very large bubbles at the distributor plate. This is observed in the fully developed churn-turbulent flow regime.

The gas hold-up results in Figure 5 show that the gas hold-up profiles in the carbon-demineralized water slurries show an increase, whereas in Figure 6, the silica-demineralized water slurries show a slight decrease when compared with the gas hold-up profiles in the nonslurry-demineralized water system. One of the prime effects of the catalyst particles in the slurry phase is increasing the slurry density and the slurry viscosity. This effect is prominent above 5 vol %,[37,38] which leads to a decrease in the gas hold-up. Another catalyst particle property which is of importance is its wetting characteristic which has a strong influence on the coalescing behavior of the bubbles, depending on the particle being hydrophobic or hydrophilic.[39,40] This effect is more pronounced at lower particle concentrations, that is, below 5 vol %. A schematic diagram is shown in Figure 10 to illustrate the influence of the carbon and silica particles on the bubble coalescence behavior just above the distributor when the growing bubble collides with the leading bubble.

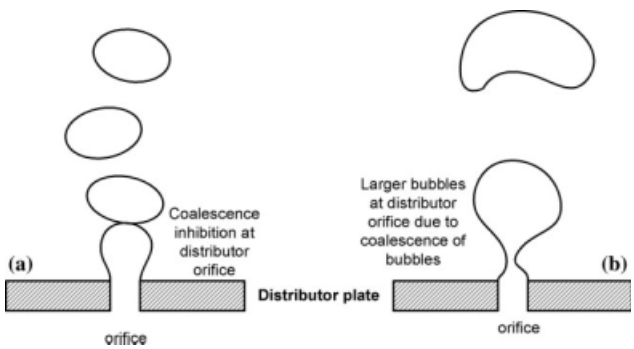


**Figure 9. Formation of gas bubbles in case of noncoalescing and coalescing gas–liquid system at the orifice of the gas distributor.**

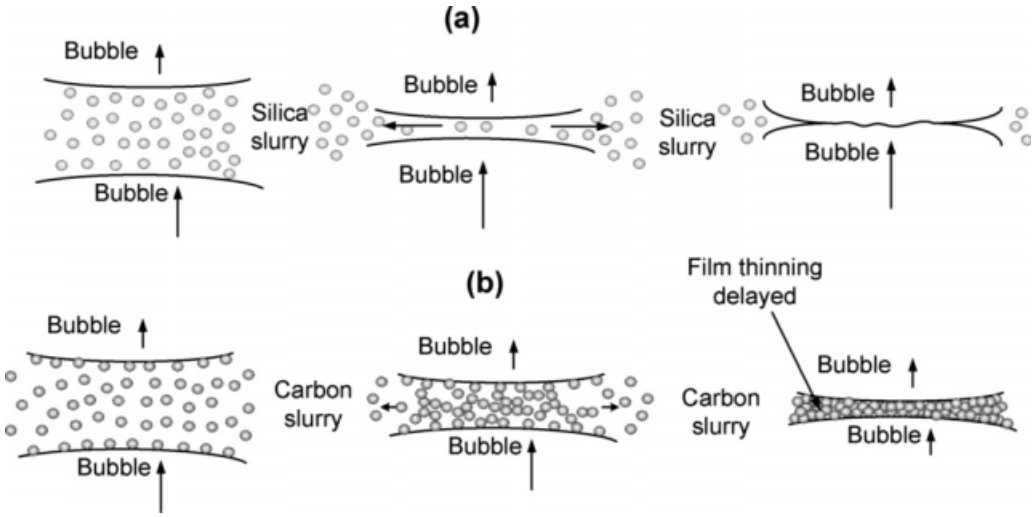


**Figure 10. Schematic representation of the coalescence of two small bubbles in demineralized water in the presence of (a) hydrophilic silica particles and (b) hydrophobic activated carbon particles.**

The coalescence of small bubbles above the distributor plate follows three distinct steps after they collide, viz., film formation, film drainage, and film rupture.[39–41] The film drainage is the rate limiting step in the complete sequence of bubble coalescence. In Figure 10a, the coalescence of bubbles in the silica-demineralized water slurry is shown. Silica particles primarily stay in the bulk of the liquid phase due to their hydrophilicity and a negligible amount of particles stays at the gas–liquid interface. As the two rising bubbles collide in the slurry, a film is formed between the two bubbles and the silica particles move away from the gas–liquid interface towards the bulk liquid. The particles drag some liquid from the film along with it, helping in faster thinning and draining of the film. The film also develops ripples or disturbances due to the outward movement of the silica particles from the film to the bulk liquid. This induces faster rupture of the film leading to enhanced coalescence and smaller coalescence times than in the case of pure demineralized water. Thus silica particles increase the rate of coalescence. In Figure 10b, the coalescence of bubbles in the presence of carbon slurries is shown schematically. Hydrophobic activated carbon particles attach to the gas–liquid interface of the bubbles.[29,42] As the bubbles collide, a film is formed between the two bubbles. In this film, the activated carbon particles remain at the gas–liquid interface and make the film rigid. The activated carbon particles resist the drainage of the film making it immobile and increasing the film drainage time. The larger film drainage time decreases the coalescence rate of the bubbles. Thus activated carbon particles decrease the coalescence rate of small bubbles when compared with the rate of coalescence in pure demineralized water.

The particle size distribution also influences the coalescence rate to some extent. The activated carbon particles are influenced by the liquid flow and the degree of turbulence around the bubbles. Small particles have a longer residence time at the gas–liquid interface and they prevail mainly in the wake of the rising bubbles. The larger particles or particle agglomerates stay in the bulk of the liquid phase and are hardly present at the gas–liquid interface. During the coalescence, mostly the trailing bubble collides with the leading bubble, thus the collision takes place in the wake of the leading bubble where small particles of carbon are present. The activated carbon particles still have the same influence of making the liquid film between the bubbles immobile and thus decreasing the coalescence rate as in case of the stationary system as described earlier. The silica particles are always in the liquid bulk and hardly at the gas–liquid interface. Hence, the particle size distribution of silica particles does not influence the increased coalescence of bubbles observed due to the presence of silica particles.

### *Average large bubble diameter*

The average large bubble diameter was estimated by using the pressure fluctuations technique as described by Chilekar et al.[31] According to this technique, the incoherent standard

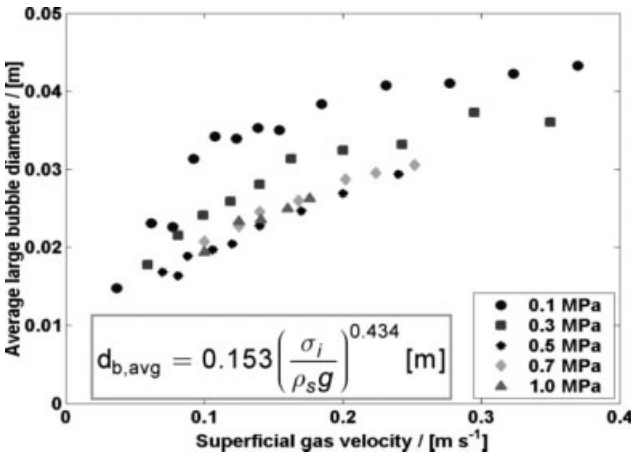


**Figure 11. Average large bubble diameter at different elevated pressures. $N_2$-demineralized water system was used.**

The equation was developed by Chilekar et al.[31] to measure average bubble diameter as a function of incoherent standard deviation ($\sigma_i$) of measured pressure fluctuations in the bubble column.

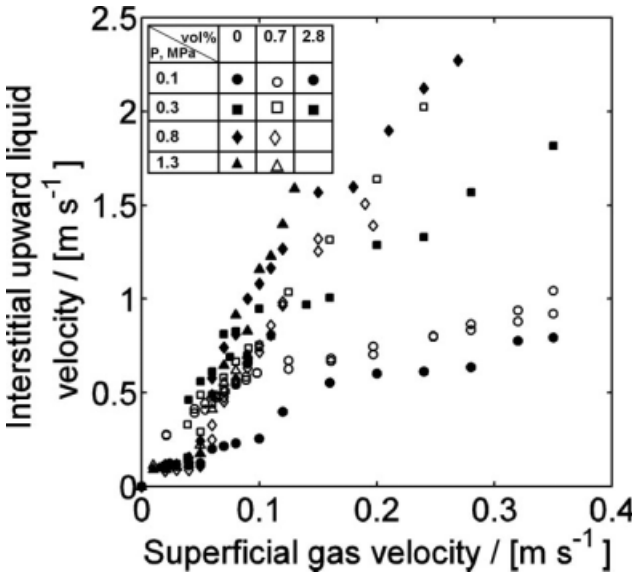


**Figure 12. Interstitial centerline upward liquid velocity at different elevated pressures.**

$N_2$-demineralized water system used with carbon slurry particles.

deviation obtained from the spectral analysis of the dynamic pressure fluctuations measured in the column is used to determine the average large bubble diameter. The average large bubble diameter was calculated for the demineralized water nonslurry system at superficial gas velocities higher than the regime transition velocity at pressures of 0.1, 0.3, 0.5, 0.7, and 1.0 MPa, as shown in Figure 11.

At 0.1 MPa pressure, the average large bubble diameter increases sharply to around 0.04 m at a superficial gas velocity just above the regime transition velocity of $u_{trans} = 0.02$ m s$^{-1}$. At higher gas velocities, the average large bubble diameter increases slightly with the superficial gas velocity over the range of velocities investigated. At higher operating pressure, that is, greater than 0.3 MPa, the average large bubble diameter decreases for the same superficial gas velocity. With increasing operating pressure, the break-up rate of the large bubbles increases due to the increased gas density. Letzel et al.[11] used the Kelvin-Helmholtz stability criterion to explain the increase in break-up of the large gas bubbles at higher operating pressure. This leads to a smaller equilibrium size of the bubbles as can be seen in Figure 11. At operating pressure higher than 0.5 MPa, there was no further significant decrease in the average large bubble diameter.

The results in this sub-section show that the large bubble diameter can be easily determined using the pressure fluctuations technique also for bubble columns operated at elevated pressure. The only limitation for the use of this technique is the availability of pressure transducers which have a sufficiently large pressure range for measuring at higher pressure and also a stable response at high operating pressure. The accuracy of the sensors needs to be about 50–100 Pa.

### *Centerline liquid velocity*

The interstitial centerline liquid velocity measured for the aqueous silica slurries at elevated pressure is shown in Figure 12. The interstitial liquid velocity showed a remarkable influence of operating pressure. With increase in pressure for demineralized water, the interstitial liquid velocity increased significantly as seen in Figure 12. At 0.1 MPa, with increase in slurry concentration from 0 vol % to about 2.8 vol % of silica, there is a slight increase in the interstitial liquid velocity. At high pressures, the average bubble size decreases due to the high break-up rate of the large bubbles. This leads to a decrease in the bubble rise velocity and hence an increase in the gas hold-up. From Eq. 1, it is seen that as the gas hold-up increases the interstitial liquid velocity also increases, as seen in Figure 12. Similar trends in the interstitial liquid velocity were obtained for silica-Isopar M and carbon-Isopar M systems.

### *Mass transfer coefficient*

Letzel and Stankiewicz[28] showed that for nitrogen-demineralized water at high pressure, the ratio of the mass transfer

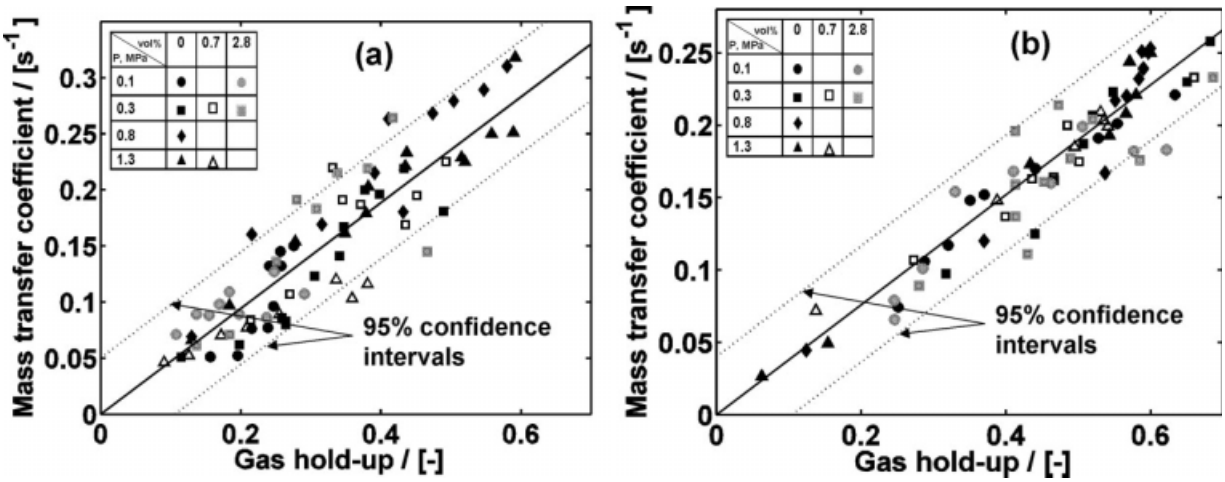


**Figure 13. Mass transfer coefficient vs. gas hold-up for slurries at various pressures: (a) silica-demineralized water slurries, (b) silica-Isopar M slurries.**

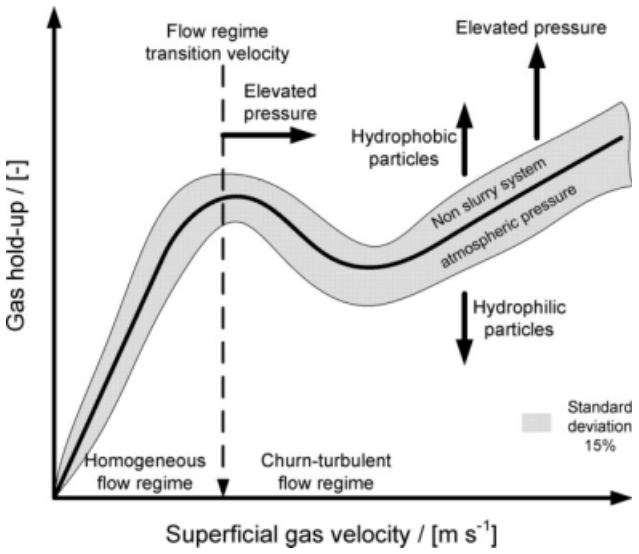


**Figure 14. Schematic representation of the gas hold-up profile in a slurry bubble column at elevated pressure and in the presence of catalyst particles.**

Vertical arrows: trends in gas hold-up profiles. Horizontal arrow: regime transition velocity trend.

coefficient to the gas hold-up ($k_l a_l/\varepsilon_g$) is approximately constant in the churn-turbulent flow regime. However, the effect of particles was not investigated by Letzel and Stankiewicz,[28] Vandu and Krishna[43] found that for silica slurries in various liquids at atmospheric pressure, this ratio is constant for slurry concentrations below 5 vol % but decreases at higher slurry concentrations. Our $k_l a_l$ vs. $\varepsilon_g$ data obtained for the silica-demineralized water slurries and for the silica-Isopar M slurries are shown in Figure 13a,b, respectively.

The solid lines represent the least-squared-residuals fit of the data, dashed lines represent the 95% confidence band. For the silica-demineralized water slurries $k_l a_l/\varepsilon_g = 0.47 \pm 0.05\ s^{-1}$, in agreement with the value of Letzel and Stankiewicz[28] for demineralized water, and for the silica-Isopar M slurries $k_l a_l/\varepsilon_g = 0.38 \pm 0.06\ s^{-1}$.

### *Mass transfer correlation*

Higbie's theory[35] states that $Sh = 1.13\ Re^{0.5}\ Sc^{0.5}$, with $Sh = k_l d_b/D$, $Re = \rho_l d_b u_b/\mu_l$, and $Sc = \mu_l/\rho_l D$. It is important to note that the equations derived in this work are for the oxygen case; however, they can be generally applicable for other gas–liquid systems with the appropriate diffusion coefficient and other physical properties. With $a_l/\varepsilon_g = 6/d_b$ for spherical bubbles, the equation for $k_l a_l/\varepsilon_g$ then becomes:

$$\frac{k_l a_l}{\varepsilon_g} = 1.13 \frac{6}{d_b} \left[\frac{u_b D}{d_b}\right]^{0.5} s^{-1} = 6.8 \sqrt{\frac{D u_b}{d_b^3}}\ s^{-1} \qquad (2)$$

Predominantly, small gas bubbles determine the value of $k_l a_l/\varepsilon_g$ for they provide for most of the gas–liquid interfacial area; a gas bubble of 3 mm has a 10 times higher specific interfacial area than a gas bubble of 3 cm. For Isopar M, the bubble diameter at the distributor plate is ~2.5 mm.[44] The rise velocity of these gas bubbles is 0.17 m $s^{-1}$.[45] Substituting these values in Eq. 2 gives a $k_l a_l/\varepsilon_g$-value of 0.83 $s^{-1}$, a factor 2.2 higher than the experimental value of 0.38 $s^{-1}$. Because $k_l a_l/\varepsilon_g$ is constant, apparently, the average gas bubble diameter does not change significantly with gas velocity or particle concentration. The same holds for the demineralized water data. The bubble diameter at the distributor plate is ~3 mm[44] with a rise velocity of 0.17 m $s^{-1}$.[45] Equation 2 predicts a $k_l a_l/\varepsilon_g$-value of 1.08 $s^{-1}$, a factor 2.3 higher than the experimental value of 0.47 $s^{-1}$. Incorporating the average of this experimental factor of 2.25 in Eq. 2 results in the following correlation:

$$\frac{k_l a_l}{\varepsilon_g} = 3.0 \sqrt{\frac{D u_b}{d_b^3}}\ s^{-1} \qquad (3)$$

with $d_b$ the diameter of the gas bubbles at the sparger estimated from Kulkarni and Joshi,[44] and $u_b$ determined from the equation by Wesselingh.[45] It is important to note that Eq. 3 is only validated for the churn-turbulent flow regime, for operating pressures between 0.1 and 1.3 MPa and for slurry concentrations up to 3 vol %.

## Concluding Remarks

The effects of operating pressure and presence of low concentrations of slurry particles on the gas hold-up profiles in a slurry bubble column are schematically represented in Figure 14. At elevated pressure, the higher gas density leads to the faster bubble disengagement at the orifice on the distributor plate into smaller bubbles than at atmospheric pressure. These small gas bubbles are stable and need significant liquid circulation rates for coalescence into larger bubbles. Thus the regime transition at elevated pressure occurs at superficial gas velocities higher than at atmospheric pressure. The gas hold-up correspondingly increases in the churn-turbulent flow regime and this increases the performance of the slurry bubble columns at elevated pressure giving a higher volumetric mass transfer coefficient. The lyophobicity of the catalyst particle decides the further increase or decrease of the gas hold-up. Thus the overall hydrodynamic behavior of the SBC is based on a combined influence of the pressure and the catalyst particles lyophobicity. The key results are listed below:

(1) The gas hold-up and the flow regime transition point are not influenced by the presence of lyophilic particles at low slurry concentrations up to 3 vol %. Lyophobic particles shift the regime transition to a higher gas velocity and induce foaming.

(2) The regime transition velocity increases with operating pressure. The average large bubble diameter decreases with pressure in the nonslurry demineralized water system.

(3) The interstitial liquid velocity increases with pressure and at a given pressure it increases with increasing slurry concentration.

(4) The gas–liquid mass transfer coefficient is proportional to the gas hold-up for all investigated slurries and is not affected by the particle lyophobicity nor by the elevated operating pressure.

(5) The ratio of the mass transfer coefficient to the gas hold-up for silica-demineralized water slurries is obtained as

$k_l a_l/\varepsilon_g = 0.47 \pm 0.05\ s^{-1}$. For silica-Isopar M slurries, this ratio is obtained as $k_l a_l/\varepsilon_g = 0.38 \pm 0.06\ s^{-1}$.

(6) The ratio $k_l a_l/\varepsilon_g$ for a particular gas–liquid–solid system in a bubble column can be estimated using the system's appropriate physical properties as $k_l a_l/\varepsilon_g = 3.0\sqrt{Du_b/d_b^3}\ s^{-1}$.

## Acknowledgments

The authors gratefully acknowledge the Dutch Technology Foundation STW, DSM Research BV, Akzo Nobel Central Research, Shell Global Solutions International BV, and Sasol Technology Netherlands BV for their financial support, and Engelhard De Meern BV and Norit NV for supplying the catalyst particles.

## Notation

$a_l$ = interfacial area per unit volume of liquid, $m^{-1}$
$d_b$ = average bubble diameter at the sparger ($d_b = 6d_o/\rho_l g$), m
$d_o$ = diameter of the orifice at the sparger, m
$d_p$ = mean particle diameter, $\mu$m
$D$ = diffusivity of gas phase in liquid, $m^2\ s^{-1}$
$\Delta H$ = heat of immersion, mJ $m^{-2}$
$k_l a_l$ = liquid side mass transfer coefficient per unit volume of the liquid, $s^{-1}$
$k_l$ = intrinsic mass transfer coefficient of the liquid side, m $s^{-1}$
$m$ = constant in the Rice and Geary[32] equation, dimensionless
$M_A$, $M_B$ = molecular weight, kg $kmol^{-1}$
$P_c$ = critical pressure, MPa
$\Delta P$ = pressure drop, Pa
$r$ = variable in the radial direction, m
$R$ = radius of the column, m
$Re$ = Reynolds number ($Re = \rho_l d_b u_b/\mu_l$), dimensionless
$S_{BET}$ = BET surface area of catalyst particles, $m^2\ g^{-1}$
$Sc$ = Schmidt number ($Sc = \mu_l/\rho_l D$), dimensionless
$Sh$ = Sherwood number ($Sh = k_l d_b/D$), dimensionless
$T_c$ = critical temperature, K
$u_b$ = bubble rise velocity of the gas bubbles formed at the sparger ($u_b = 0.71\sqrt{gd_b}$), m $s^{-1}$
$u_g$ = superficial gas velocity, m $s^{-1}$
$v_A$ = molar volume of gases, $m^3\ kmol^{-1}$
$V_l$ = interstitial centerline liquid velocity, m $s^{-1}$
$V_{s,p}$ = pore volume of catalyst particles, ml $g^{-1}$

### *Greek letters*

$\varepsilon_g$ = overall gas hold-up, $m^3_{gas}\ m^{-3}_{reactor}$
$\varepsilon_{g,r}$ = radial gas hold-up, $m^3_{gas}\ m^{-3}_{reactor}$
$\varepsilon_p$ = porosity of the particles, $m^3_{gas}\ m^{-3}_{particle}$
$\mu_l$ = viscosity of slurry, Pa s
$\rho_l$ = density of slurry, kg $m^{-3}$
$\rho_s$ = solid density of particles, kg $m^{-3}$

## Literature Cited

1. Krishna R, Ellenberger J, Hennephof DE. Analogous description of the hydrodynamics of gas-solid fluidized beds and bubble columns. *Chem Eng J*. 1993;53:89–101.
2. Krishna R, Ellenberger J. Gas holdup in bubble column reactors operating in the churn-turbulent flow regime. *AIChE J*. 1996;42:2627–2634.
3. Behkish A, Men Z, Inga JR, Morsi BI. Mass transfer characteristics in a large-scale slurry bubble column reactor with organic liquid mixtures. *Chem Eng Sci*. 2002;57:3307–3324.
4. Dewes I, Schumpe A. Gas-density effect on mass transfer in the slurry bubble column. *Chem Eng Sci*. 1997;52:4105–4109.
5. Idogawa K, Ikeda K, Fukuda T, Morooka S. Effect of gas and liquid properties on the behavior of bubbles in a column under pressure. *Int Chem Eng*. 1987;27:93–99.
6. Jiang P, Lin T-J, Luo X, Fan L-S. Flow visualisation of high pressure (21MPa) bubble column: bubble characteristics. *Trans IChemE*. 1995;73:269–274.
7. Jordan U, Terasaka K, Kundu G, Schumpe A. Mass transfer in high-pressure bubble columns with organic liquids. *Chem Eng Tech*. 2002;25:262–265.
8. Kojima H, Sawai J, Suzuki H. Effect of pressure on volumetric mass transfer coefficient and gas holdup in bubble column. *Chem Eng Sci*. 1997;52:4111–4116.
9. Lau R, Peng W, Velazquez-Vargas LG, Yang GQ, Fan L-S. Gas-liquid mass transfer in high-pressure bubble columns. *Ind Eng Chem Res*. 2004;43:1302–1311.
10. Lemoine R, Behkish A, Morsi BI. Hydrodynamics and mass-transfer characteristics in organic liquid mixtures in a large-scale bubble column reactor for toluene oxidation process. *Ind Eng Chem Res*. 2004;43:6195–6212.
11. Letzel HM, Schouten JC, Krishna R, van den Bleek CM. Characterization of regimes and regime transitions in bubble columns by chaos analysis of pressure signals. *Chem Eng Sci*. 1997;52:4447–4459.
12. Oyevaar MH, de la Rie T, van der Sluijs CL, Westerterp KR. Interfacial areas and gas hold-ups in bubble columns and packed bubble columns at elevated pressures. *Chem Eng Proc*. 1989;26:1–14.
13. Oyevaar MH, Bos R, Westerterp KR. Interfacial areas and gas hold-ups in gas-liquid contactors at elevated pressures from 0.1 to 8.0 MPa. *Chem Eng Sci*. 1991;46:1217–1231.
14. Pohorecki R, Moniuk W, Zdrojkowski A. Hydrodynamics of a bubble column under elevated pressure. *Chem Eng Sci*. 1999;54:5187–5193.
15. Reilly IG, Scott DS, De Bruijn TJW, MacIntyre D. The role of gas phase momentum in determining gas holdup and hydrodynamic flow regimes in bubble column operations. *Can J Chem Eng*. 1994;72:3–12.
16. Stegeman D, Knop PA, Wijnands AJG, Westerterp KR. Interfacial area and gas holdup in a bubble column reactor at elevated pressures. *Ind Eng Chem Res*. 1996;35:3842–3847.
17. Tarmy B, Chang M, Coulaloglou C, Ponzi P. Hydrodynamic characteristics of three phase reactors. *Chem Eng*. 1984;407:18–23.
18. Urseanu MI, Guit RPM, Stankiewicz A, van Kranenburg G, Lommen JHGM. Influence of operating pressure on the gas hold-up in bubble columns for high viscous media. *Chem Eng Sci*. 2003;58:697–704.
19. Vafopulos I, Sztatescsny K, Moser F. Der einfluss des partial-und gesamtdruckes auf den stoffaustausch. *Chem Eng Tech*. 1975;47:681–786.
20. Wilkinson PM, Haringa H, Van Dierendonck LL. Mass transfer and bubble size in a bubble column under pressure. *Chem Eng Sci*. 1994;49:1417–1427.
21. Yang GQ, Fan LS. Axial liquid mixing in high-pressure bubble columns. *AIChE J*. 2003;49:1995–2008.
22. Behkish A, Lemoine R, Sehabiague L, Oukaci R, Morsi BI. Gas holdup and bubble size behavior in a large-scale slurry bubble column reactor operating with an organic liquid under elevated pressures and temperatures. *Chem Eng J*. 2007;128:69–84.
23. Deckwer W-D, Louisi Y, Zaidi A, Ralek M. Hydrodynamics of Fischer-Tropsch slurry reactor. *Ind Eng Chem Proc Des Dev*. 1980;19:699–708.
24. Inga JR, Morsi BI. Effect of operating variables on the gas holdup in a large-scale slurry bubble column reactor operating with an organic liquid mixture. *Ind Eng Chem Res*. 1999;38:928–937.
25. Luo X, Lee DJ, Lau R, Yang GQ, Fan L-S. Maximum stable bubble size and gas holdup in high-pressure slurry bubble column. *AIChE J*. 1999;45:665–680.
26. Tinge JT, Rodriguez Casado AJ. Influence of pressure on the gas hold-up of aqueous activated carbon slurries in a down flow jet loop reactor. *Chem Eng Sci*. 2002;57:3575–3580.
27. Ruthiya KC, Chilekar VP, Warnier M, van der Schaaf J, van Ommen JR, Kuster BFM, Schouten JC. Detecting regime transitions in slurry bubble columns using pressure time series. *AIChE J*. 2005;51:1951–1965.
28. Letzel HM, Stankiewicz A. Gas hold-up and mass transfer in gas-lift reactors operated at elevated pressures. *Chem Eng Sci*. 1999;54:5153–5157.
29. Ruthiya KC, van der Schaaf J, Kuster BFM, Schouten JC. Model to describe mass-transfer enhancement by catalyst particles adhering to a gas-liquid interface. *Ind Eng Chem Res*. 2005;44:6123–6140.
30. Thorat BN, Shevade AV, Bhilegaonkar KN, Aglawe RH, Veera UP, Thakre SS, Pandit AB, Sawant SB, Joshi JB. Effect of sparger

design and height to diameter ratio on fractional gas hold-up in bubble-columns. *Chem Eng Res des*. 1998;76:823–834.
31. Chilekar VP, Warnier MJF, van der Schaaf J, van Ommen JR, Kuster BFM, Schouten JC. Bubble size estimation in slurry bubble columns from pressure fluctuations. *AIChE J*. 2005;51: 1924–1937.
32. Rice RG, Geary NW. Prediction of liquid circulation in viscous bubble columns. *AIChE J*. 1990;36:1339–1348.
33. Letzel HM, Schouten JC, van den Bleek CM, Krishna R. Influence of elevated pressure on the stability of bubbly flows. *Chem Eng Sci*. 1997;52:3733–3740.
34. Kluytmans JHJ, van Wachem BGM, Kuster BFM, Schouten JC. Gas holdup in a slurry bubble column: influence of electrolyte and carbon particles. *Ind Eng Chem Res*. 2001;40:5326–5333.
35. Ruthiya KC, van der Schaaf J, Kuster BFM, Schouten JC. Influence of particles and electrolyte on gas hold-up and mass transfer coefficient in a slurry bubble column. *Int J Chem React Eng*. 2006;4:A13.
36. Vrij A, Overbeek JT. Rupture of thin liquid films due to spontaneous fluctuations in thickness. *J Am Chem Soc*. 1968;90:3074–3078.
37. Vandu CO, Krishna R. Influence of scale on the volumetric mass transfer coefficient in bubble columns. *Chem Eng Proc*. 2004;43:575–579.
38. Krishna R, De Swart JWA, Ellenberger J, Martina GB, Maretto C. Gas holdup in slurry bubble-columns - effect of column diameter and slurry concentrations. *AIChE J*. 1997;43:311–316.
39. Prince MJ, Blanch HW. Bubble coalescence and break-up in air-sparged bubble columns. *AIChE J*. 1990;36:1485–1499.
40. Marrucci G. A theory of coalescence. *Chem Eng Sci*. 1969;24:975–985.
41. Deckwer W-D. *Bubble Column Reactors*. Chichester: John Wiley & sons, 1992.
42. van der Zon M, Hamersma PJ, Poels EK, Bliek A. Coalescence of freely moving bubbles in water by the action of suspended hydrophobic particles. *Chem Eng Sci*. 2002;57:4845–4853.
43. Vandu CO, Krishna R. Volumetric mass transfer coefficients in slurry bubble columns operating in the churn-turbulent flow regime. *Chem Eng Proc*. 2004;43:987–995.
44. Kulkarni AA, Joshi JB. Bubble formation and bubble rise velocity in gas-liquid systems: a review. *Ind Eng Chem Res*. 2005;44:5873–5931.
45. Wesselingh JA. The velocity of particles, drops, and bubbles. *Chem Eng Proc*. 1987;21:9–14.

*Manuscript received Mar. 31, 2009, and revision received May 23, 2009.*